Author Accepted Manuscript (AAM). This manuscript is made available under the Creative Commons Attribution-NonCommercial-NoDerivatives 4.0 International (CC BY-NC-ND 4.0) license (https://creativecommons.org/licenses/by-nc-nd/4.0/).
Please cite the final published version in Renewable Energy via the DOI/ScienceDirect link

Degradation and Projected Lifetime of Polycrystalline Silicon Photovoltaic Modules After 10 Years of Field Exposure in the Atacama Desert

Abstract

This study quantifies degradation and projects the useful lifetime of polycrystalline silicon photovoltaic modules operating in the Atacama Desert, using I–V measurements taken after ten years of field exposure. The methodology included a visual inspection, outdoor I–V curve measurements, STC correction by IEC 60891 standard, and the evaluation of four key parameters V_{oc}, I_{sc}, P_{mpp}, and FF by comparing 2024 data with initial manufacturer specifications and ten long-term field studies conducted in comparable desert climates. Statistical analysis of the large-sample dataset (64 strings encompassing 1,216 modules) yielded a mean degradation rate of 1.32%/year in P_{mpp}, corresponding to a projected lifetime of 15.15 years to the 80% power threshold, while a sensitivity analysis of realistic commissioning-time deviations in the initial power broadens the degradation rate to the range 0.87–1.58%/year and the associated lifetime to approximately 13–23 years. Common failure modes included cell cracking as an irreversible structural failure at the cell level, and environmental soiling as an optics-driven loss mechanism affecting the module frontsheet. These results emphasise the need for operation and maintenance strategies adapted to Atacama conditions and provide an STC-normalised benchmark that can support reliability assessment and warranty evaluation of PV plants in hyper-arid and other high-irradiance desert environments.

Keywords: Crystalline silicon, Atacama Desert, Photovoltaic degradation, STC correction, I–V characteristic curve

1. Introduction

During the past two years, worldwide photovoltaic capacity (PV) has experienced significant expansion, reaching an installed capacity of 1,406.7 gigawatts (GW) in 2023 and 1,858.6 GW in 2024 [1], primarily driven by the dominance of crystalline silicon (c-Si) PV technologies, which remain the leading choice on the market, representing 98% in 2024 [2]. The Chilean government proposed the target to reduce greenhouse gas emissions by 30% below 2007 levels by 2030 [3]. To achieve this, Chile has reached an operationally installed PV capacity exceeding 6.4 GW in 2023; concurrently, around 44.1 GW were planned for addition, with approximately 4.9 GW already under construction [4].

Most solar power plants are located in the north-central region of Chile due to the significant impact of the Atacama Desert. Considered the driest desert in the world, it experiences an annual solar irradiation that exceeds 2,700 kW h/m^2 [5]. Characterised by its high-altitude areas and exceptionally arid conditions, it leads to the highest levels of solar radiation worldwide [6]. One of the critical concerns is the harsh climate, which significantly affects the encapsulant materials, leading to the degradation of c-Si PV modules after prolonged exposure [7].

Assessing the performance of PV modules is crucial for comparing it with the degradation rates declared in the warranty. Manufacturers usually provide a 25-year power warranty characterised by two distinct zones, as shown in Figure 1. The linear warranty promises 90% of the nominal maximum power by the 10th year, whereas the stepped warranty ensures 80% by the 25th year. In the initial year, the warranty datasheet typically specifies an allowable 3% of the nominal power loss [8]. The output power is specified in the datasheet under Standard Test Conditions (STC), defined by irradiance G_{STC} = 1,000 W/m^2 and cell temperature T_{STC} = 25 °C, as stated in the International Electrotechnical Commission (IEC) 60904-3 standard [9]. However, STC does not reflect the full range of degradations that occur in real outdoor environments, particularly in regions with extreme climatic stressors.

The degradation results from the complex interaction between environmental stressors and material-specific vulnerabilities. As summarised in Figure A1 (Appendix A), mechanical (e.g., wind, hail, installation stress), thermal (irradiance and elevated temperature), chemical (H_2O, O_2, and corrosive species), and electrical stressors act on the components of the PV module, triggering chemical reactions such as corrosion or bond scission. These processes lead to diverse failure modes, including cell cracking, potential-induced degradation (PID), and delamination, which ultimately manifest as reduced current, power losses, and safety risks such as hotspots or arcing [10]. For conceptual clarity, this study uses the term ‘degradation modes’ in a broad sense to describe observable manifestations that lead to performance losses, including both phenomena driven by environmental stressors and structural failures.

The discrepancy between STC and outdoor conditions has motivated the development of climate-specific modelling approaches to improve the prediction of real-world behaviour [11]. Consequently, evaluating the long-term performance of PV modules remains a complex but essential task to complement warranty-based expectations and improve the design, maintenance, and reliability assessment of PV systems in diverse operating environments. To address this challenge, the scientific literature categorises the performance metrics for evaluating the degradation of PV technologies into four main groups [8]: (1) electrical parameters obtained from the current-voltage relationship

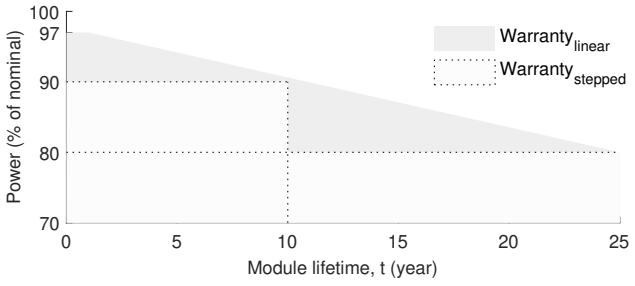

Figure 1. Degradation through the lifetime of a typical c-Si PV module.

Nomenclature

Acronyms

BWh	Hot desert climate
BWk	Cold desert climate
IEC	International Electrotechnical Commission
IRT	Infrared Thermography
PV	Photovoltaic
STC	Standard Test Conditions
UV	Ultraviolet

Symbols

α	Temperature coefficient for I_{sc} (A/°C)
β	Temperature coefficient for V_{oc} (V/°C)
$\bar{X}$	Mean value
σ	Standard deviation value
a	Irradiance correction factor (dimensionless)
$CI_{95\%}$	95% confidence interval
D_X	Degradation (%)
DR_X	Degradation rate (%/year)
FF	Fill Factor (dimensionless)
G	Irradiance (W/m^2)
I	Current (A)
I_{mpp}	Current at maximum power point (A)
I_{sc}	Short-circuit current (A)
LD	Degradation limit of P_{mpp} (%)
n	Number of I–V curves
P_{mpp}^{eff}	Effective STC power (W)
P_{mpp}	Power at the maximum power point (W)
R_s	Series resistance (Ω)
SE	Standard error (%)
t	Exposure time (year)
t_L	Useful lifetime (year)
V	Voltage (V)
V_{mpp}	Voltage at maximum power point (V)
V_{oc}	Open-circuit voltage (V)

Other symbols

c-Si	Crystalline silicon
m-Si	Monocrystalline silicon
p-Si	Polycrystalline silicon

Subscripts

0	Initial STC reference condition
1	Measured condition
2	Corrected condition

(I–V) measured in outdoor or indoor environments and corrected to STC; (2) regression models such as Photovoltaics for Utility Scale Applications (PVUSA), Photovoltaic Geographical Information System (PVGIS) and Sandia models; (3) normalised ratings such as P_{mpp}/P_{max}, P_{AC}/P_{max} and kWh/kWp.

The first group, particularly the outdoor I–V curve measurements, has been extensively used. Manufacturers provide five key electrical parameters identified on the I–V curve under STC: open-circuit voltage V_{oc}, maximum power point P_{mpp}, short-circuit current I_{sc}, voltage V_{mpp} and current I_{mpp} at the maximum power point. Figure 2 illustrates the normalised I–V (green) and power-voltage (P–V) (magenta) curves, P_{mpp} is reached for the coordinate points (V_{mpp}, I_{mpp}). Five key electrical parameters are highlighted by points and a dashed rectangular area that helps to calculate the fill factor (FF) in Equation (1) [12].

$$FF = \frac{V_{mpp} \cdot I_{mpp}}{V_{oc} \cdot I_{sc}} \quad (1)$$

By definition, FF is a dimensionless quantity in the [0,1] interval or as a percentage. A practically efficient conversion process in c-Si modules is generally associated with $FF \gtrsim 0.7$, however, $FF = 1$ is not physically attainable [13].

The mentioned definitions establish the measurement framework adopted here, which includes I–V curves and metrics derived from their electrical parameters. The key contributions are summarised as follows:

- Document the main degradation modes through a visual inspection campaign.
- Conduct a statistical analysis of cumulative degradation for four key electrical parameters (V_{oc}, I_{sc}, P_{mpp} and FF) using I–V curves measured after 10 years of outdoor exposure in a grid-connected PV plant located in the Atacama Desert. This analysis leverages one of the largest STC-corrected datasets reported for hyper-arid desert conditions, enabling the quantification of degradation trends and variability in c-Si modules.

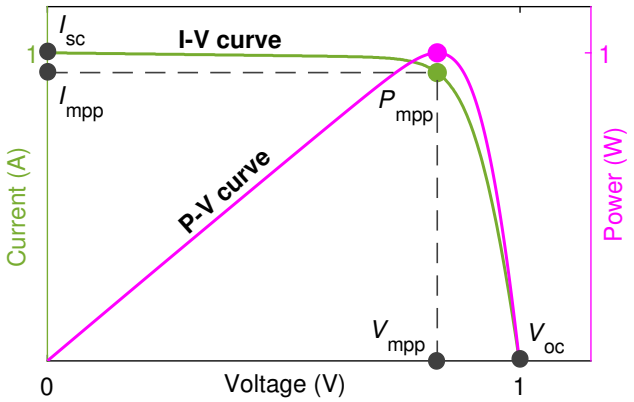

Figure 2. Normalised characteristic curves observed in c-Si PV modules.

- Provide a comparative assessment of the implications concerning warranty expectations and earlier studies conducted in desert climates.

The paper is structured as follows: Section 2 synthesises evidence on PV performance in Atacama and other desert-climate studies; Section 3 describes the characteristics of the PV plant studied, the instrumentation, the dataset, and the methodology used; Section 4 presents and discusses the main findings, offering a detailed comparison with manufacturer data and the literature; finally, Section 5 provides concise conclusions from degradation and reliability analysis.

2. Literature review

Key research in the Atacama Desert focusses on PV technology performance and soiling effects, with Ferrada et al. [14] linking soiling composition to local microclimate and deposition mechanisms,

and Olivares et al. [15] assessing the impacts of desert dust and operational variability. Dust characterisation studies by Ferrada et al. [14] identified saline-fine particulates and cementation on module frontsheets, while Olivares et al. [16] studied the microstructural cementation and its climatic drivers. Additionally, Cordero et al. [17] quantified sub-regional soiling losses, and Tobosque et al. [18] provided spatially resolved data on performance penalties to inform maintenance scheduling.

By Köppen-Geiger Photovoltaic Climate classification [19], Atacama Desert is classified as a BWk (cold desert) climate, whereas other desert sites fall into the BWh (hot desert). Studies conducted in BWk climates have been documented, such as Fezzani et al. [20] which determined the degradation rate of 2%/year in m-Si modules after 10 years of exposure in Algeria. Bayandelger [21] reported degradation rates of 1%/year for m-Si modules and 1.3%/year for p-Si modules over 14 years in Mongolia; the leading cause of the decrease in P_{mpp} was identified as the reduction in I_{sc}, mainly attributed to dust accumulation on the frontsheet. Mahammed et al. [22] examined the degradation of three PV systems over 11 years in Algeria; the results showed a higher degradation rate for m-Si modules (1.53%/year) than for p-Si modules (0.37%/year). Huang et al. [23] analysed the degradation and reliability evaluation of the c-Si modules installed in China over 7 years. It proposed a relationship between power guarantee, degradation rate, and tolerance of P_{mpp} over 30 years. Dahesh et al. [24] evaluated the degradation of c-Si modules after 38 years of operation in Yemen, revealing a median power degradation of 0.77%/year.

Similarly, in BWh climates Kahoul et al. [25] demonstrated that the degradation of the p-Si modules was significantly higher than that of m-Si modules after 6 to 11 years of operation in Algeria. Hassan Daher et al. [26] revealed a degradation rate of 0.70–0.74%/year, consistent with PR estimates of 1.0%/year, while standard PTC showed non-significant trends. Bouaichi et al. [27] evaluated for 36 months the early degradation of 76 modules in Morocco, reporting average annual power decrease rates of 2.6%/year (m-Si), 1.45–3.41%/year (p-Si, according to the manufacturer data), 2.21%/year (micromorph) and 0.05%/year (CIS). Adothu et al. [28] recently conducted an extensive review of degradation modes affecting c-Si PV modules in 11 different desert environments and proposed a novel testing protocol.

The methodologies identified in the literature are: measurements of I–V curves in outdoor/indoor environments; visual inspection; and advanced diagnostic techniques such as Infrared Thermography (IRT), Ultraviolet Fluorescence (UVF), insulation tests, and Electroluminescence (EL) imaging. Particularly in Atacama Desert, the degradation analyses leveraging I–V-corrected curves as primary performance metrics remain scarce.

3. Materials and methods

3.1. Framework for degradation analysis

Since no commissioning-time outdoor/indoor I–V measurements were available for this PV plant, the nominal STC power was adopted as the initial reference data. However, the impact of this assumption was subsequently quantified through a sensitivity analysis (Section 4.4). Accordingly, the four-step methodology illustrated in Figure 3 was adopted.

The first step involved a field visual inspection campaign. The second step involved measuring the outdoor I–V curves, ensuring accuracy by cleaning the selected PV modules before conducting the measurements. The third step involved STC-corrected I–V curves, according to the IEC 60891 standard [29]. Finally, the fourth step encompassed statistical analysis and degradation assessment, including (i) estimation

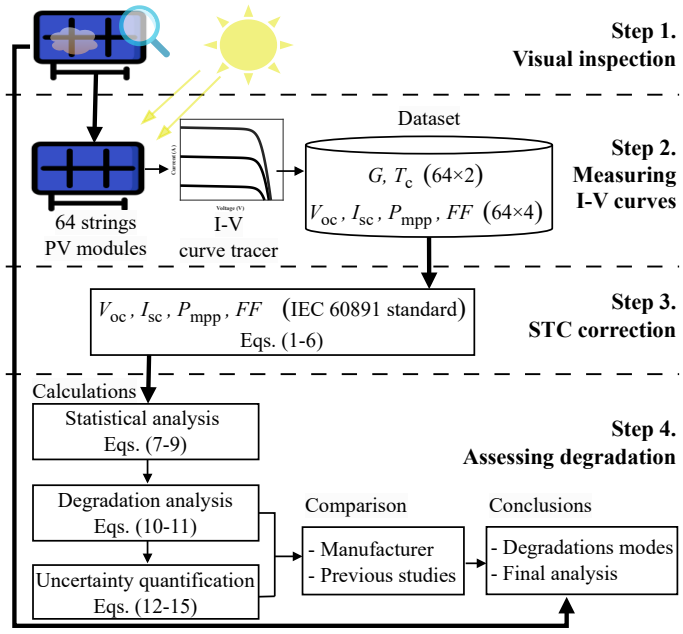

Figure 3. Framework of the four-step methodology used for degradation analysis.

of cumulative and annualised degradation of STC–corrected parameters after 10 years of exposure, (ii) calculation of mean values, standard deviations, and standard errors, (iii) linear trend fitting to derive degradation rates, and (iv) uncertainty quantification through confidence intervals and extrapolated module lifetimes. Then, these results were compared with the initial manufacturer specifications and similar case studies.

3.2. Characteristics of the PV plant and modules

The solar power plant is a grid-connected PV system located in Atacama Desert (Figure 4a) and was commissioned in 2014. It features a mechanical solar tracking system that optimises the tilt angle, ensuring maximum reliability and accuracy in the collected data. The system includes SunEdison p-Si modules, each consisting of 72 series-connected solar cells. Under STC, the nominal parameters are P_{mpp} = 305 W ± 3 %, V_{oc} = 45.29 V, V_{mpp} = 35.77 V, I_{sc} = 8.95 A, I_{mpp} = 8.53 A. The temperature coefficient of I_{sc} is α = 0.044,75 A/°C, and for V_{oc} is β = −0.149,45 V/°C.

3.3. Visual inspection procedure

A structured *ad hoc* visual inspection campaign was carried out as the first step of the methodology. The campaign had a dual purpose: (i) to document the dominant degradation modes across the PV plant and (ii) to pre-select modules without severe visible defects for subsequent electrical characterisation. Each module was examined for frontsheet, frame, and cell defects, including cell cracks, glass breakage, delamination, encapsulant discolouration, junction-box damage, and visible soiling. Two trained inspectors walked all accessible rows and screened approximately 2,000 modules, recording the presence or absence of each defect type and modules with any damage for exclusion from measurements. PV strings containing modules with any defects were excluded from I–V measurement dataset to avoid biassing the statistical analysis. Finally, 64 strings (each with 19 series-connected modules) from the pool of visually accepted were then selected, totalling 1,216 PV modules.

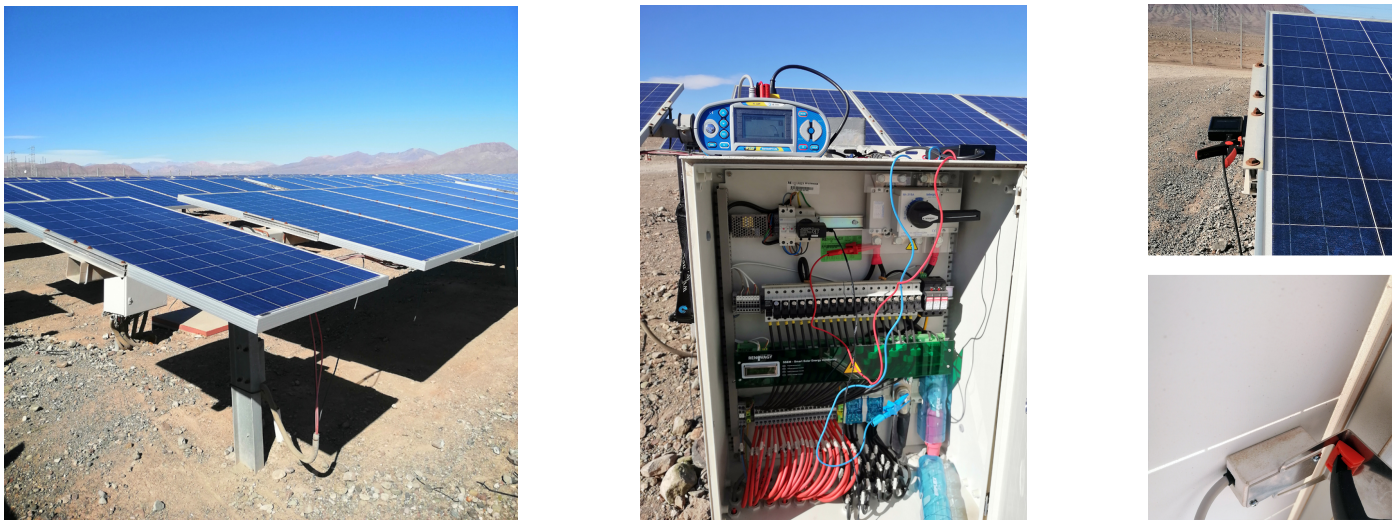

(a) (b) (c)

Figure 4. Overview of (a) PV strings operating in Atacama Desert, (b) I–V curve tracer connected to the junction-box and (c) sensors of irradiance (top) and cell temperature (bottom) connected to a PV string.

3.4. Instrumentation and data collection

The MI 3109 EurotestPV Lite instrument (Figure 4b) was used. Table 1 provides the technical specifications. The device includes the tests required by the IEC 60891 standard [29] to characterise PV modules/strings by obtaining the I–V curve and subsequently converting the measured maximum power to nominal STC power.

Table 1. Technical specifications of the I–V curve tracer.

Parameter	Measuring range	Resolution	Accuracy
Voltage	0 – 999 V	1 V	±1%
Current	0 – 15 A	0.01 A	±1%
Power	0 – 15 kW	10 W	±2%
Irradiance	0 – 2,000 W/m^2	1 W/m^2	±4%+5 digits
Temperature	-10 °C – +85 °C	0.1 °C	±5 digits

Measurements were taken between October 1st and 4th, 2024 (Chilean spring), under clear-sky conditions. The curve tracer was connected between 2:00 PM and 3:00 PM when irradiance exceeded $G > 900\,\mathrm{W/m^2}$. Cell temperature was measured with a sensor attached to the backsheet for tight contact (Figure 4c, bottom), and the irradiance was measured with a sensor placed parallel to the frontsheet (Figure 4c, top).

3.5. Data processing

The dataset is structured as a 64×6 matrix, divided into 64×4 for electrical and 64×2 for climate-related parameters, as shown in the second step of Figure 3. The data processing adopted here complies with IEC 60891 [29] and aligns with studies reported in BWk climates [20, 22], which facilitate comparisons with both manufacturer specifications and published results.

3.5.1. Correcting I–V curves to STC

Through Equations (2)-(6) the IEC 60891 standard provides a robust procedure to minimise uncertainties in I–V curve measurements. It enables the extrapolation of the measured data of PV modules/strings to STC, normalising the results (of outdoor conditions) for direct comparison with nominal values. Furthermore, the procedure reduces the impact of fluctuations in irradiance and non-standard temperatures, thereby enhancing the consistency and comparability of the results. In addition, the electrical parameters (Section 3.2) specified in the datasheet are required.

$$I_{sc,2} = I_{sc,1} \cdot \frac{G_2}{G_1} \cdot \left[1 + \alpha \cdot (T_2 - T_1)\right] \tag{2}$$

$$V_{oc,2} = V_{oc,1} \cdot \left[1 + a \cdot ln\left(\frac{G_2}{G_1}\right) + \beta \cdot (T_2 - T_1)\right] \tag{3}$$

$$I_2 = I_1 \cdot \frac{I_{sc,2}}{I_{sc,1}} \tag{4}$$

$$V_2 = V_1 + (V_{oc,2} - V_{oc,1}) + R_s \cdot (I_2 - I_1) \tag{5}$$

$$P_{mpp,2} = V_2 \cdot I_2 \tag{6}$$

where subscripts 1 and 2 denote the measured and corrected values. T_1 and T_2 (°C) are the measured and reference cell temperatures, respectively. G_1 and G_2 (W/m^2) are the measured and reference irradiances, respectively. α (A/°C) and β (V/°C) are the temperature coefficients for I_{sc}, V_{oc}, respectively. a is an irradiance correction factor (dimensionless), used to account for the logarithmic dependence of V_{oc} on irradiance. $a = 1$ was adopted for the p-Si modules measured above 900 W/m^2. R_s is the series resistance (Ω). FF_1 and FF_2 are calculated by Equation (1), for the measured and corrected curves, respectively.

3.5.2. Degradation and uncertainty calculations

A statistical framework is used to quantify degradation and its associated uncertainty from the I–V curves, which are assumed to be a statistically representative sample of the entire PV plant. The degradation rates are reported to two decimal places to facilitate statistical comparison; however, their absolute accuracy is limited by the specifications of the I–V curve tracer listed in Table 1. A Gaussian probability density function (Equation (7)) was used to model the dispersion of electrical parameters (V_{oc}, I_{sc}, P_{mpp}, and FF), validated by the approximately unimodal distributions observed in the histograms of Section 4.2. Mean values ($\overline{X}$, Equation (8)) and standard deviations (σ, Equation (9)) were calculated to assess central tendency and variability, minimising sampling biases.

$$p(X, \overline{X}, \sigma, t) = \frac{1}{\sqrt{2\pi}\sigma(t)} \exp\left[-\frac{(X - \overline{X}(t))^2}{2\sigma^2(t)}\right] \quad (7)$$

$$\overline{X}(t) = \frac{1}{n}\sum_{i=1}^{n} X_i(t) \quad (8)$$

$$\sigma(t) = \sqrt{\frac{1}{n}\sum_{i=1}^{n}[X_i(t) - \overline{X}(t)]^2} \quad (9)$$

where, X is a random variable describing the values of electrical parameters (e.g. V_{oc}, I_{sc}, P_{mpp}, or FF), t is the exposure time (year), $X(t)$ is the value of one of the electrical parameters at time t, $i \in \{1, 2, \ldots, n\}$ with n representing the total number of I–V curves.

Equations (10) and (11) were used to calculate degradation $D_{\overline{X}}$ (%) and the degradation rate $DR_{\overline{X}}$ (%/*year*), which quantify the relative loss in values of electrical parameters due to outdoor exposure [23].

$$D_{\overline{X}} = \frac{X(0) - \overline{X}(t)}{X(0)} \cdot 100 \quad (10)$$

$$DR_{\overline{X}} = \frac{D_{\overline{X}}}{t} \quad (11)$$

where, $X(0)$ is the value of the electrical parameter X at the initial time $t = 0$ (considered the first year of PV plant commissioning).

Statistical precision was reached by computing the standard error of the mean degradation ($SE_{D_{\overline{X}}}$, Equation (12)) and the annualised degradation rate ($SE_{DR_{\overline{X}}}$, Equation (13)), with 95% confidence intervals ($CI_{95\%}$, Equation (14)) using a t-distribution critical value of 1.998 for $n = 64$. This methodology supports reliable degradation estimates for reliability modelling and warranty validation in desert conditions.

$$SE_{D_{\overline{X}}} = \frac{\sigma}{\sqrt{n}} \quad (12)$$

$$SE_{DR_{\overline{X}}} = \frac{SE_{D_{\overline{X}}}}{t} \quad (13)$$

$$CI_{95\%} = \overline{X}_{DR} \pm t_{\alpha/2,n-1} \cdot SE_{DR_{\overline{X}}} \quad (14)$$

The suitability of the Gaussian distribution was validated using a Kolmogorov–Smirnov test applied to the measured values of V_{oc}, I_{sc}, P_{mpp} and FF, yielding p-values of 0.2483, 0.4608, 0.8050, and 0.0605, respectively.

Based on the manufacturer warranty in Figure 1, the useful life of the c-Si PV modules was estimated using Equation (15) [30].

$$t_L = \frac{100\% - LD}{DR_{\overline{X}}} \quad (15)$$

where, t_L is the useful life (*year*) and LD is the degradation limit (%) of P_{mpp}. Typically, the latter parameter is specified in the datasheet by $LD = 80\%$.

4. Results and discussions

4.1. Visual inspection

Primary degradation modes were identified, such as cracked cells detected sporadically in several modules, with a random distribution (Figure 5a), dust accumulation affecting the entire PV module population (Figure 5b), and isolated bird droppings observed in only four modules, indicating a minimal occurrence (Figure 5c). In contrast, dust accumulation was observed across almost all visually inspected modules, representing a widespread degradation mode. These findings align with prior studies in arid climates around the world, as summarised in Table 2. Dust accumulation and cracked cells are commonly reported, while bird droppings, although less frequent, also represent a risk to PV performance [31, 21].

4.2. Analysing the measured I–V and P-V curves

Figure 6 shows the 64 curves, including measured (red), STC–corrected (blue) and the manufacturer reference (green). The maximum power points are marked by circles. Their relative displacement visually illustrates the cumulative degradation effects and the partial compensation achieved through STC correction. The progressive reduction in rectangular areas (delineated by dashed lines) further confirms the long-term decline in FF. The manufacturer's curve is considered the first year of solar plant commissioning studied under STC. It serves as a baseline for assessing degradation over time. The application of Equations (2)-(6) successfully extrapolated the measured data to STC. Each I–V curve was measured within an irradiance range of $G_{min,1} = 920\,W/m^2$ and $G_{max,1} = 964\,W/m^2$. The mean irradiance was $\overline{G_1} = 946.64\,W/m^2$, with $\sigma_{\overline{G_1}} = 10.51\,W/m^2$. Similarly, the temperature varied within $T_{min,1} = 46.9\,°C$ and $T_{max,1} = 55.7\,°C$. The mean temperature was $\overline{T_1} = 52.41\,°C$ and $\sigma_{\overline{T_1}} = 2.36\,°C$.

During the measurement, G_1 levels were observed close to standard irradiance ($G_2 = G_{STC} = 1{,}000\,W/m^2$), while T_1 levels were significantly higher, exceeding twice the standard temperature ($T_2 = T_{STC} = 25\,°C$). Figure 6a shows that the measured I_{sc} values are relatively unaffected by elevated values of T_1 due to their strong dependence on G_1, whereas V_{oc} drops significantly at higher temperatures T_1. Similarly, Figure 6b reveals that P_{mpp} was reduced due to the combined effects of decreased voltage and a slight reduction in current.

The decline in PV performance illustrated in Figure 6, aligns with expectations resulting from the cumulative impacts of long-term exposure, as listed in Table 2. Although the STC–corrected curves show improved values compared to the measured curves, the key points of the I–V curve still fall below the original manufacturer's parameters. Therefore, despite standardisation, a significant loss in the primary key electrical parameters remains on the I–V curve. The findings show that the environmental stressors affect not only the PV performance but also the long-term reliability of the solar plant.

The statistical summary in Table 3 illustrates the disparity between the values of four key electrical parameters for the measured, STC–corrected, and manufacturing curves. The data obtained from the PV strings were normalised by dividing the voltage of each PV string by 19; which is practical since the initial performance listed in the datasheet is specified per module. V_{oc} decreased from 45.29 V to 44.57 V in STC–corrected, representing a degradation of 1.61%. Similarly, I_{sc} dropped from 8.95 A to 8.19 A, reflecting a degradation of 8.45%, primarily attributed to long-term optics-related losses (e.g., cementation and frontsheet transmittance degradation).

Table 2. Summary of the three degradation modes identified in this study and previously reported in the Atacama Desert and other desert regions.

Degradation modes	Reference, Atacama	Reference, Country
Cracked cells	[31, 32]	[21], Mongolia [24], Yemen [33], Qatar [34], Morocco
Dust accumulation	[31, 15–18]	[35], Algeria [36], Saudi Arabia [37], MENA*
Bird droppings	[31, 15]	[22], Algeria

*Countries located in the Middle East and North Africa.

(a) (b) (c)

Figure 5. Degradation modes such as (a) cell crack, (b) dust accumulation, and (c) bird droppings observed on the PV modules.

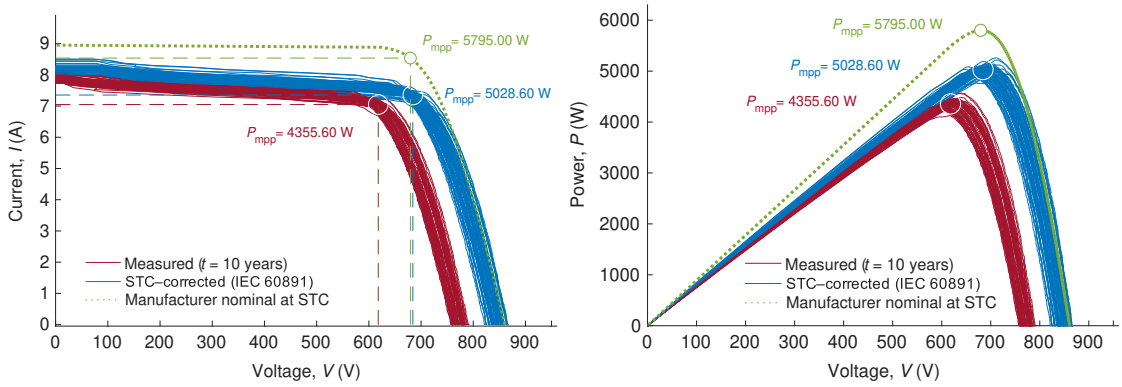

(a) (b)

Figure 6. Characteristic curves of 64 PV strings after 10 years of operation: (a) I–V and (b) P–V. Measured (red), STC–corrected (blue), the manufacturer reference (green) curves and their respective P_{mpp} points (circle) are shown. Dashed lines delineate the rectangular areas used to compute FF.

P_{mpp} exhibited the highest degradation of 13.22%, reducing from 305 W to 264.66 W in STC–corrected. The variability of P_{mpp} values is modest ($\sigma(10) = 4.44$ W), suggesting that the selected strings form a relatively homogeneous subset. FF also decreased in STC–corrected, showing a reduction of 3.60%. Since FF exceeded 70%, the PV performance can be considered acceptable, with consistently stable I–V curves.

4.3. Assessing the degradation of key electrical parameters

Figure 7 illustrates the histograms along with their Gaussian distributions for each parameter. V_{oc} and FF show low degradation, while the most significant degradation occurred in I_{sc} and P_{mpp}, which is consistent with the main stressors in harsh environments, such as dust accumulation, causing optical deterioration. The shape of the histograms suggests that degradation processes have occurred uniformly, validated by the Kolmogorov-Smirnov tests, which confirm the suitability of the Gaussian assumption. This uniformity provides a reliable foundation for evaluating long-term performance [23].

Table 4 summarises the degradation rates of four electrical parameters, statistically derived using Equations (8)–(14). Manufacturers typically report maximum degradation rates of $DR_{P_{\text{mpp}}} \leq 1\%$/year in the 10th year and $DR_{P_{\text{mpp}}} \leq 0.5\%$/year between the 10th and 25th year of operation [30], as shown in Figure 1. In contrast, the data in Table 4 reveal that after 10 years of outdoor exposure, the cumulative degradation of P_{mpp} reaches a value of 13.22%, corresponding to a mean annual degradation rate of 1.32%. Significant degradation in I_{sc} (mean 8.45%, $\sigma = 1.26\%$) is identified as the main contributor to

Table 3. Statistical summary of four key electrical parameters obtained from the measurements after 10 years, STC–corrected and the manufacturer reference.

		Individual module				String of 19 series-connected modules			
Data	Parameter	V_{oc} (V)	I_{sc} (A)	P_{mpp} (W)	FF (%)	V_{oc} (V)	I_{sc} (A)	P_{mpp} (W)	FF (%)
Measured (t = 10 years)	$\overline{X}$	40.77	7.93	229.24	70.92	774.67	7.93	4,355.60	70.92
	σ	0.47	0.09	4.07	0.85	8.85	0.09	77.39	0.85
STC–corrected (IEC 60891)	$\overline{X}$	44.57	8.19	264.66	72.49	846.81	8.19	5,028.60	72.49
	σ	0.60	0.11	4.44	0.84	11.42	0.11	84.39	0.84
Manufacturer reference at STC	X	45.29	8.95	305.00	75.20	860.70	8.95	5,795.00	75.20

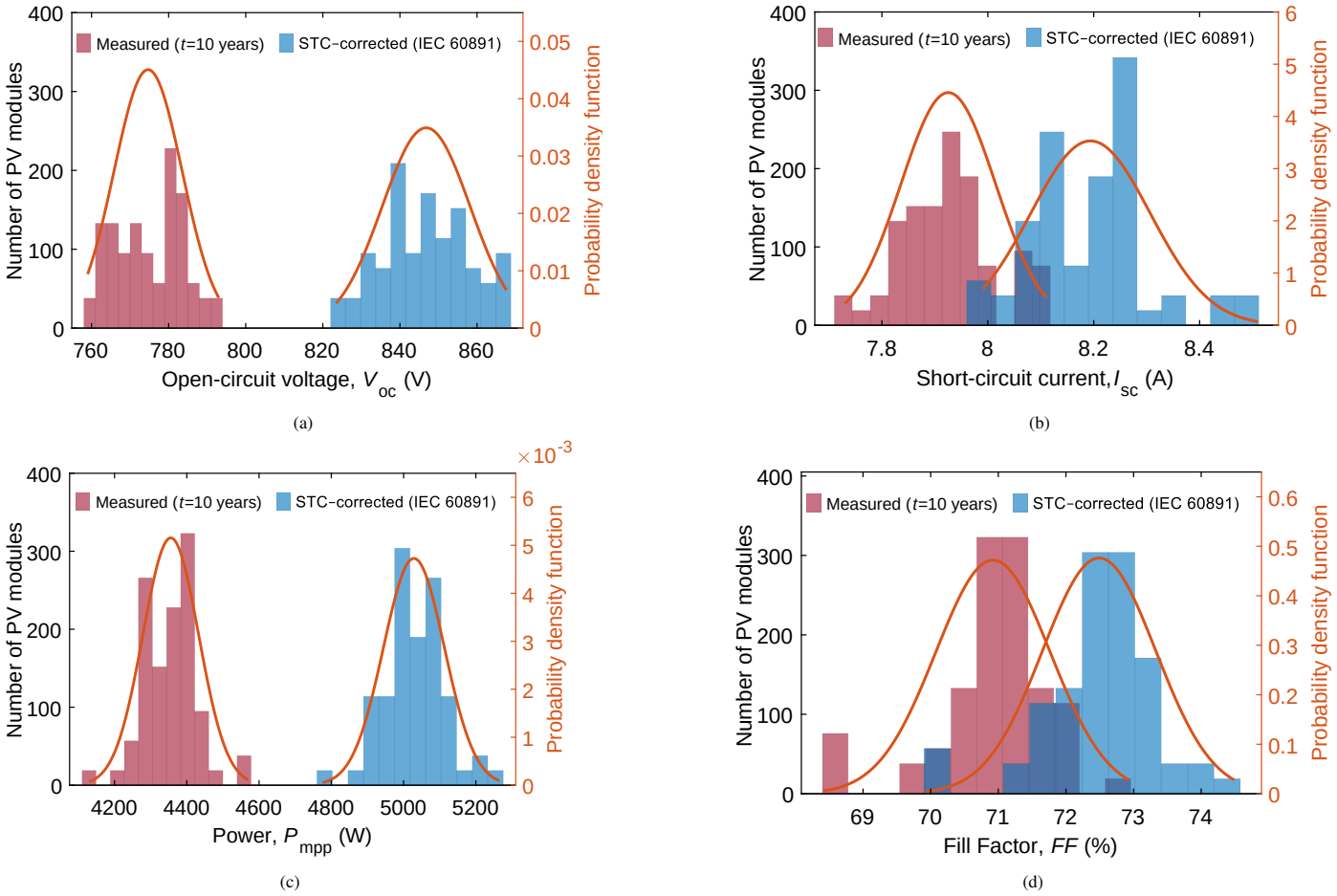

Figure 7. Distributions between measured and STC–corrected for (a) V_{oc}, (b) I_{sc}, (c) P_{mpp}, and (d) FF, after 10 years of exposure in the Atacama Desert.

the reduction in P_{mpp}, which subsequently impacts FF (mean 3.60%, σ = 1.11%). The narrow confidence intervals and low standard errors (e.g., $SE_{DR_{\bar{Y}}} = 0.02$ for P_{mpp}) indicate high precision in these estimates, reinforcing the reliability of the observed trends despite the challenging environmental conditions.

Based on Equation (15) and the mean performance degradation rate, the expected lifetime of the PV modules is illustrated in Figure 8. The green curves delineate the linear warranty, specifying 80% power retention at 25 years and 90% at 10 years. The red dashed line represents the degradation after a 10-year period and indicates an outdoor exposure lifetime of 15.15 years. The dotted red line shows lifetime estimates ranging from 14.81 to 15.50 years. These results are consistent with observations by Bouaichi et al. [34], Osterwald and McMahon [30], who reported a linear decline in PV module output power over long-term exposure.

Analysing the narrow confidence intervals (Figure 8) under the

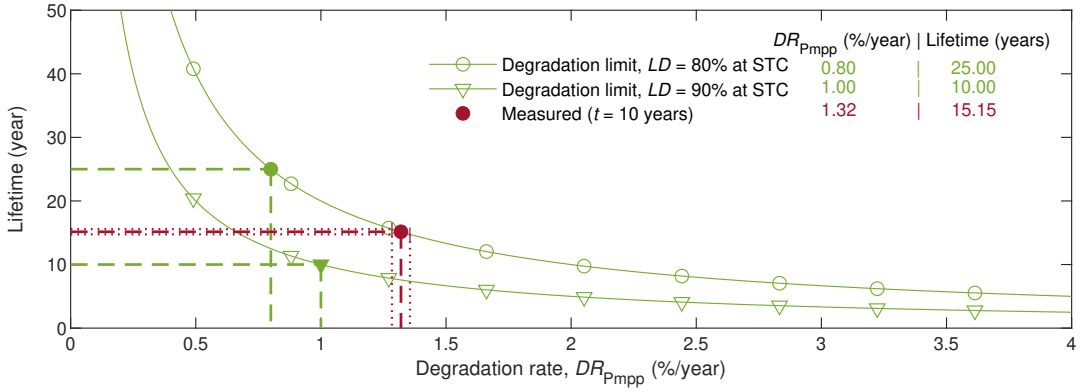

Figure 8. Expected lifetime as a function of $DR_{P_{mpp}}$ with uncertainty bands. The solid green lines represent degradation limits of 80% and 90% at STC, while the dashed lines and points indicate measured and manufacturer reference degradation rates. The dotted lines depict $CI_{95\%}$ = 1.29–1.36%/year, with a corresponding lifetime of t_L = 14.81–15.50 years.

Table 4. Statistical summary of degradation of four key electrical parameters.

Degradation	Parameter	V_{oc}	I_{sc}	P_{mpp}	FF
$D_{\overline{x}}$ (%)	max	4.33	10.73	17.58	7.01
	min	0.82	4.92	9.15	0.94
	$\overline{X}$	1.61	8.45	13.22	3.60
	σ	1.33	1.26	1.46	1.11
$DR_{\overline{X}}$ (%/year)	$\overline{X}$	0.16	0.84	1.32	0.36
	$SE_{DR_{\overline{X}}}$	0.02	0.02	0.02	0.01
	$CI_{95\%}$	0.13–0.19	0.80–0.87	1.29–1.36	0.33–0.39

assumed nominal STC power at commissioning, the linear warranty will be satisfied within the initial 15.15 years. However, projecting this trend linearly over the remaining 9.85 years to reach the 25-year warranty period yields a cumulative degradation of approximately $D_{P_{mpp}} = 33\%$ (i.e., $1.32\% \cdot 25$), exceeding the guaranteed 20% loss threshold ($LD = 80\%$ (green curve with a solid circle). This discrepancy highlights a significant deviation from the datasheet projections, underscoring unexpectedly pronounced declines in power performance beyond the manufacturer specifications.

4.4. Sensitivity analysis of initial nominal STC power

The absence of *in situ* I–V curve measurements during the first year of operation prevents a direct determination of the initial power, therefore, long-term degradation analysis must account for missing or incomplete baseline information [38]. In addition, recent field-based studies have quantified deviations between the STC nominal power and the effective STC power inferred from *in situ* measurements. For example, in a PV plant in Spain, the inferred nominal power after 10 years of exposure showed a deficit of approximately 5% relative to STC [39]. In contrast, for a grid-connected plant in Peru, the effective power rating inferred from field measurements was nearly 7% lower than the nominal STC power, mainly due to module mismatch, resistive wiring losses and spectral differences with respect to the AM1.5 reference spectrum [40]. These cases illustrate that the nominal STC power used for performance assessment may differ from the true effective baseline, and they motivate the sensitivity-based treatment adopted in the remainder of this section.

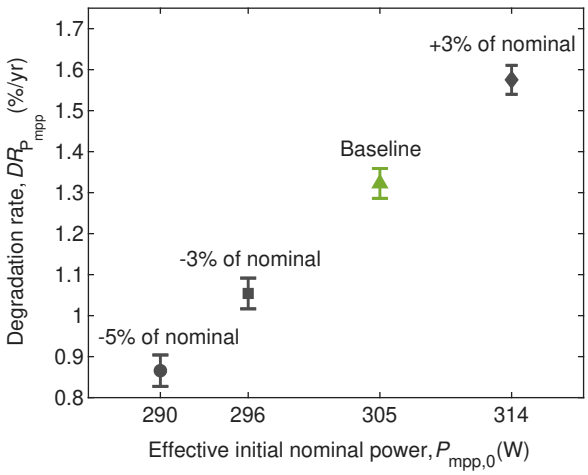

Figure 9. Degradation rate $DR_{P_{mpp}}$ as a function of the effective initial STC power $P^{eff}_{mpp,0}$ for four scenarios: spectral/mismatch/soiling (−5%), optimistic (−3%), baseline (manufacturer nominal at STC), and pessimistic (+3%). Error bars indicate the 95% confidence interval ($CI_{95\%}$) of the sample mean.

To explicitly account for this baseline uncertainty, the notation $P^{eff}_{mpp,0}$ is introduced to denote the effective initial STC power used as input to the degradation model. Thus, Equations (10)–(15) become explicit functions of $P^{eff}_{mpp,0}$, such that any perturbation in this effective baseline is analytically propagated into the estimated degradation rate and useful life. Then, $P^{eff}_{mpp,0}$ is perturbed according to four scenarios, as shown in Figure 9. The scenarios ±3% are consistent with the datasheet tolerance, while a scenario −5% is added as a conservative envelope for the effective STC power, to account for residual optical and mismatch losses not explicitly captured by the field I–V calibration. This choice is consistent with Atacama-specific evidence showing that local spectral conditions can modify the current by several percent relative to standard AM1.5 spectra, and that soiling can induce substantial power losses [41].

For each scenario, $DR(P^{eff}_{mpp,0})$ and $t_L(P^{eff}_{mpp,0})$ were recalculated using the STC–corrected values ($P_{mpp,2}$). Reducing $P^{eff}_{mpp,0}$ by −3% (optimistic scenario) lowers the estimated rate to 1.05%/year and extends the lifetime to $t_L = 19.05$ years, while increasing it by +3% (pessimistic scenario) raises the rate to 1.58%/year and shortens the lifetime to $t_L = 12.66$ years. The scenario in −5% further reduces the mean degradation rate to 0.87%/year with the expected corresponding lifetime of $t_L = 22.99$ years, which is longer than the baseline estimated in Figure 8. These results are provided in Appendix A (Table A1) to explicitly quantify how the commissioning-time uncertainties in $P^{eff}_{mpp,0}$ propagate to the degradation rate and the lifetime estimates: perturbations within ±3% to −5% broaden $DR_{P_{mpp}}$ to 0.87–1.58%/year and the associated lifetime to approximately 13 to 23 years.

4.5. Comparative analysis

To perform a reliable comparative analysis, it is essential to standardise the evaluation of PV degradation in regions with comparable climate conditions and/or PV technology. There appears to be no prior research on identical PV cell technology analysed in Section 3.2 (i.e., manufacturer, series, and model). Additionally, the limited number of research studies conducted within arid zones sharing the same climatic parameters restricts comparison. Following the review of the literature (Section 2), five studies focused on the long-term deterioration of c-Si PV modules located in the BWk climate were chosen for a comparative analysis, as shown in Table 5. In addition, these studies were selected based on their methodology, specifically those that align with the approach adopted in this research, such as using I–V curves as performance metrics, conducting visual inspections to detect degradation modes, and c-Si PV technologies.

Despite variability between manufacturers and tolerances, Table 5 shows the degradation patterns in desert climates, where each study contributes distinctly. In Gobi Desert, Bayandelger [21] analysed m-Si and p-Si PV modules for 14 years and reported a decline in P_{mpp} linked to reductions in I_{sc} consistent with glass abrasion. In Algerian Desert over 11 years, Mahammed et al. [22] reported backsheet and junction-box damage and identified encapsulant discolouration and corrosion as prevalent drivers. Over a 38-year assessment in Sana'a (Yemen), Dahesh et al. [24] attributed peak-power losses primarily to reductions in I_{sc} and documented multi-mode failures in the most affected modules. The present study analysed a large sample of 64 strings (1,216 PV modules), which substantially exceeds the sample sizes (1–100 modules) typically reported for BWh/BWk climates (Table 5). This larger dataset reduces small-sample uncertainty and enables more robust parameter-specific degradation estimates.

As can be seen, the degradation observed in the Atacama Desert aligns with the levels reported in similar arid environments, where the degradation rates range from $DR = 2.47\%$/year over 12 years

Table 5. Comparison between the findings of the present research and previous studies conducted in BWk climates.

Reference	[24]	[23]	[20]	[21]		[22]					Present study
				Case 1	Case 2	Case 1	Case 2	Case 3	Case 4	Case 5	
Desert	Sana'a	Jinchang	Ghardaia	Gobi	Gobi	Ghardaia^{+}	Ghardaia^{+}	Ghardaia^{+}	Ghardaia^{+}	Ghardaia^{+}	Atacama
Country	Yemen	China	Algeria	Mongolia	Mongolia	Algeria	Algeria	Algeria	Algeria	Algeria	Chile
Sample (PV modules)	16	100	1	1	1	10	20	25	8	8	1,216
P_{mpp} at STC (W)	37 ± 10%	245 + 3%	50	80	75	100	50	110	55	50	305 ± 3%
Exposure time (year)	38	7	12	14	14	11	11	11	11	11	10
$D_{P_{mpp}}$ (%)	29.22	5.79	29.64	18.1	15.2	17.9	21.97	20.63	5.68	15.79 – 90	13.22
$DR_{P_{mpp}}$ (%/year)	0.77	0.83 – 1.07	2.47	1.29	1.09	1.62	1.99	1.87	0.37	2.36	1.32
Manufacturer	Arco Solar	*	Jumao photonics	*	*	Isofoton	Isofoton	Isofoton	TEA500	UDTS50	SunEdison
Technology (c-Si)	m-Si	m-Si	m-Si	p-Si	m-Si	m-Si	m-Si	m-Si	p-Si	m-Si	p-Si
Key parameters	P_{mpp}	P_{mpp}	V_{oc}, I_{sc}, V_{mpp}, I_{mpp}, P_{mpp}, FF, η	V_{oc}, I_{sc}, V_{mpp}, I_{mpp}, P_{mpp}, FF	V_{oc}, I_{sc}, V_{mpp}, I_{mpp}, P_{mpp}, FF	V_{oc}, I_{sc}, P_{mpp}	V_{oc}, I_{sc}, P_{mpp}	V_{oc}, I_{sc}, P_{mpp}	V_{oc}, I_{sc}, P_{mpp}	V_{oc}, I_{sc}, P_{mpp}	V_{oc},I_{sc}, P_{mpp}, FF
Curve tracer (model)	PVKLA4.4	XJTU-9M	PVA-600	MP-160 I–V	MP-160 I–V	PVPM2540C	PVPM2540C	PVPM2540C	PVPM2540C	PVPM2540C	MI 3109
Testing condition	outdoor	outdoor	outdoor	indoor	indoor	outdoor	outdoor	outdoor	outdoor	outdoor	outdoor

*No detailed data were available in [23] and [21]. $^{+}$Climatic zone encompassing BWk and BWh regions.

[20] to DR = 0.37%/year over 11 years [22], both in the Ghardaia Desert. Furthermore, in terms of c-Si technology, the degradation rate calculated in this study closely resembles that reported by Bayandelger [21], who analysed PV modules of the same technology in the Gobi Desert over 14 years. This consistency could reinforce the reliability of the degradation trends in similar desert environments, albeit slightly higher than the manufacturer's specifications at STC.

Although most studies on PV degradation tend to focus mainly on the decline in P_{mpp}, comprehensive analyses that include additional key electrical parameters are considerably less common. In this context, Table 5 shows that two researchers investigated the same four electrical parameters examined in the present study [20, 21]. Consequently, Table 6 provides a detailed and comprehensive evaluation of the findings. The moderate values of $D_{V_{oc}}$ and D_{FF} suggest that the dominant degradation mechanisms in the Atacama Desert mainly involve optical losses. D_{FF} exhibits a moderate decrease, falling between the value reported by Fezzani et al. [20] and the lower value observed by Bayandelger [21]. Previous research conducted in Gobi [21] and Ghardaia [22] also showed a higher value of $DR_{I_{sc}}$ compared to the other parameters, which are identified as the main reasons for the decrease in power degradation, reflecting the impact of stressors (e.g., dust, UV radiation, thermal cycling) in BWk-classified climates. Although the degradation measured in this study does not reach the higher values reported in Tables 5 and 6, it still exceeds the standard warranty threshold of the initial maximum power.

4.6. Integrated discussion and implications

The PV modules analysed in this study use low-iron tempered glass in the frontsheet; therefore, the terms frontsheet and glass are interchangeably used in Figure A1. Accordingly, the plant-wide reduction in current and output power is interpreted mainly as a consequence of widespread dust accumulation and optical losses on the glass/frontsheet, while cracked cells are understood as local irreversible structural failures associated with mechanical and thermo-mechanical stressors [42] that affect only a fraction of the modules. This environmental context, where Atacama typically receives less than 6 mm/year of rainfall and thus offers very limited natural cleaning of PV modules [15], helps to understand the results summarised in Table 4.

The campaign for diagnosis relied exclusively on *ad hoc* visual inspection; therefore, latent sub-cell/interconnect defects and thermally driven anomalies may have gone undetected. As a result, three degradation modes were identified in the present study (Table 2), a relatively low number compared to other desert environments [24]. Complementing visual inspection with IRT, EL imaging, and standardised I–V measurements enables a better diagnosis of PV module degradation and improves the attribution of underlying mechanisms [43, 44]. Furthermore, Islam et al. [45] demonstrated that correlating EL with I–V curves provides a quantitative link between optical defect mapping and electrical performance losses, establishing a reliable bridge between *in situ* and laboratory conditions.

The four scenarios adopted for the effective initial STC power (Figure 9) fall within the uncertainty bands reported for effective power rating procedures applied to utility-scale PV arrays [39, 40], and therefore should be interpreted as reflecting realistic commissioning-time uncertainty rather than extreme deviations in the underlying degradation process. Sensitivity analysis shows that plausible commissioning-time uncertainties in $P^{eff}_{mpp,0}$ are explicitly propagated into the group of degradation rate and lifetime pairs (Table A1), broadening the range of $DR_{P_{mpp}}$ and generating a spread of more than ten years in the projected lifetime at the 80% power threshold (Figure 8).

Even in the most conservative scenario of the sensitivity analysis, the estimated lifetime is shorter than that provided in the linear warranty. A

Table 6. Comparison between the degradation of four key electrical parameters of the present study and previous studies conducted in BWk climates.

Reference		Technology	t (year)	Degradation (%)				Degradation rate (%/year)			
				$D_{V_{oc}}$	$D_{I_{sc}}$	$D_{P_{mpp}}$	D_{FF}	$DR_{V_{oc}}$	$DR_{I_{sc}}$	$DR_{P_{mpp}}$	DR_{FF}
[20]		m-Si	12	0.32	2.19	29.64	28.03	0.03	0.18	2.47	2.34
[21]	Case 1	p-Si	14	0.90	11.30	18.10	1.40	0.06	0.81	1.29	0.10
	Case 2	m-Si	14	2.80	10.40	15.20	1.40	0.20	0.74	1.09	0.10
Present study		p-Si	10	1.61	8.45	13.22	3.60	0.16	0.84	1.32	0.36

recent study conducted in a BWh climate within the Pacific coastal desert belt of South America reported module-level performance loss rates for c-Si technologies in the range of 0.9–1.6%/year [46]. Although site-specific conditions and performance metrics differ between sites, the similarity in the order of magnitude between the reported degradation range and the values estimated for the plant under study (0.87–1.58%/year) reinforces the plausibility of these estimates and supports their representativeness for desert environments. From a methodological standpoint, the current estimates are inferred from a single measurement campaign after 10 years of operation. Therefore, uncertainty can be reduced in future studies by repeating identical I–V characterisation campaigns after an additional operating period (e.g., 5 years) and applying a consistent IEC 60891 standard, which improves the temporal convergence of the degradation rate and reduces sensitivity to baseline assumptions, as shown for long-term datasets with missing initial references [38].

The linear warranty provided by manufacturers appears optimistic for Atacama deployments and underscores the need for stringent qualification tests and a stronger correlation between IEC accelerated ageing tests under STC and real-world measurements. Evidence from arid-desert campaigns converges on this view, but from complementary angles such as: Kahoul et al. [25] (Algeria) ties elevated losses to desert stressors and I–V parameter drift; Bouaichi et al. [27] (Morocco) quantifies above-expected losses and motivates site-tailored cleaning; Bouaichi et al. [34] shows that adding IR, EL, and outdoor I–V exposes non-visual defects that cause performance losses; and Adothu et al. [28] argues for desert-orientated test cycles beyond current IEC standards.

5. Conclusions

This study quantified the long-term degradation of polycrystalline silicon PV modules under the hyper-arid conditions of Atacama Desert, using outdoor I–V curves as the primary performance metric and providing a statistical benchmark. The observed reduction in current and power output is dominated by soiling affecting the glass/frontsheet, which induces optics-driven losses and appears as a sustained decline in I_{sc} with only moderate changes in V_{oc} and FF. Meanwhile, thermo-mechanical stressors leading to cell cracking constitute a secondary and irreversible degradation mode.

The annual degradation rate in output power lies within a plausible range of 0.87 to 1.58%, estimating a useful lifetime of roughly 13 to 23 years at the power threshold of 80%. Even under the most conservative scenario, these values are higher than those implied by typical linear warranty assumptions, indicating that standard manufacturer guarantees are optimistic for hyper-arid desert deployments.

The findings imply that PV plants operating in BWk/BWh climates should explicitly prioritise strategies that preserve the optical path and limit soiling-related losses, alongside careful monitoring of current and power trends as primary indicators of degradation. At the same time, they support the need for reliability assessments and warranty schemes that are explicitly tailored to desert climates rather than extrapolated from moderate-condition test protocols.

The analysis is constrained by the focus on a single PV plant and the absence of advanced diagnostic techniques for detailed failure attribution. Future work should combine outdoor I–V measurements in commissioning-time with indoor STC characterisation and integrate infrared thermography, electroluminescence, and multi-site monitoring in Atacama to refine degradation models and reduce systematic uncertainty in long-term lifetime projections.

Appendix A

Declaration of Competing Interest

The authors declare that they have no known competing financial interests or personal relationships that could have appeared to influence the work reported in this paper.

Data availability

The generated and analysed dataset is not publicly available due to confidentiality agreements with the solar plant operator, but anonymised data are available from the corresponding author upon request.

Acknowledgements

The authors acknowledge funding from the bilateral research project DIE23-0001 (WBI/AGCID RI02). The authors also appreciate the support provided by the National Research and Development Agency (ANID) through the FONDECYT Regular grant number 1220556 and SERC Chile FONDAP 1523A0006. Additional funding was provided by the Research Project PINV01-743 of the National Council of Science and Technology (CONACYT). Furthermore, the authors acknowledge the International Research Collaboration Fund 2024-2025 from the University of Nottingham A7C200.

References

[1] IRENA, Renewable capacity statistics 2025, International Renewable Energy Agency, Abu Dhabi, 2025. URL: https://www.irena.org/Publications/2025/Mar/Renewable-capacity-statistics-2025, [Online, Accessed on March 26, 2025].

[2] M. Fischer, M. Woodhouse, T. Brammer, P. Baliozian, International Technology Roadmap for Photovoltaics (ITRPV) – 2024 Results (2025). 16th Edition, April 2025.

[3] S. Nasirov, P. Gonzalez, J. Opazo, C. Silva, Development of Rooftop Solar under Netbilling in Chile: Analysis of Main Barriers from Project Developers' Perspectives, Sustainability 15 (2023). doi:10.3390/su15032233.

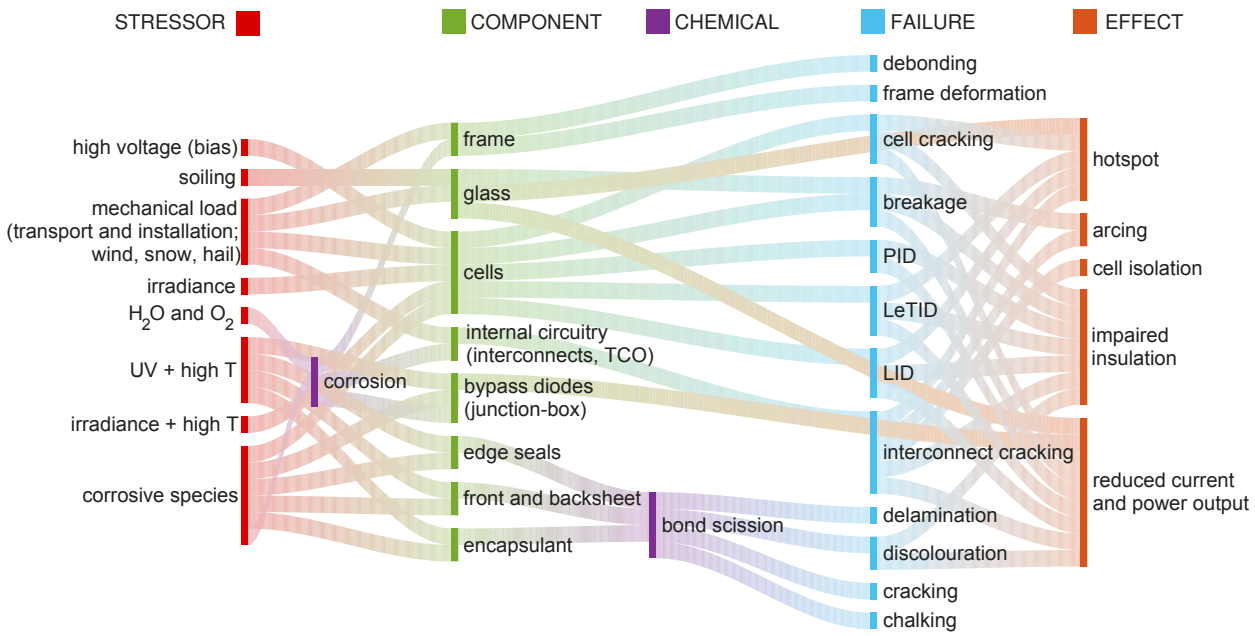

Figure A1. Diagram representing the relationships between stressor, component, failure and effect. Acronyms: UV: ultraviolet radiation; TCO: transparent conductive oxide; PID: potential-induced degradation; LID: light-induced degradation; LeTID: light- and elevated-temperature-induced degradation. Corrosive species refer to chemically reactive environmental agents, including acid rain, acetic acid vapors, salt mist, and ammonia, which induce electrochemical corrosion, hydrolysis, and polymer degradation in PV encapsulant, edge seals, and metallic interconnects. Adapted from [10].

Table A1. Sensitivity of the degradation rate and projected lifetime to assumptions on the effective initial STC power.

Scenario	$P^{\text{eff}}_{\text{mpp},0}$ (W)	t_L (year)	$DR_{P_{\text{mpp}}}$ (%/year)	$CI_{95\%}$ (%/year)
Spectral/mismatch/soiling (−5% of nominal)	289.75	22.99	0.87	0.83–0.90
Optimistic (−3% of nominal)	295.85	19.05	1.05	1.02–1.09
Baseline (manufacturer nominal at STC)	305.00	15.15	1.32	1.29–1.36
Pessimistic (+3% of nominal)	314.15	12.66	1.58	1.54–1.61

[4] CNE, Solar photovoltaic (PV) generation capacity in Chile in January 2023, by project stage (in megawatts), 2023. URL: https://www.statista.com/statistics/1206670/solar-pv-capacity-chile-stage/, [Online, Accessed on April 20, 2025].

[5] D. Icaza-Alvarez, F. Jurado, M. Tostado-Véliz, Smart energy planning for the decarbonization of Latin America and the Caribbean in 2050, Energy Reports 11 (2024) 6160–6185. doi:10.1016/j.egyr.2024.05.067.

[6] A. Zurita, A. Castillejo-Cuberos, M. García, C. Mata-Torres, Y. Simsek, R. García, F. Antonanzas-Torres, R. A. Escobar, State of the art and future prospects for solar PV development in Chile, Renewable and Sustainable Energy Reviews 92 (2018) 701–727. doi:10.1016/j.rser.2018.04.096.

[7] B. Menacer, N. E. H. Baghdous, S. Narayan, M. Al-lehaibi, L. Osorio, V. Tuninetti, Efficiency Enhancement of Photovoltaic Panels via Air, Water, and Porous Media Cooling Methods: Thermal–Electrical Modeling, Sustainability 17 (2025). doi:10.3390/su17146559.

[8] A. Phinikarides, N. Kindyni, G. Makrides, G. E. Georghiou, Review of photovoltaic degradation rate methodologies, Renewable and Sustainable Energy Reviews 40 (2014) 143–152. doi:10.1016/j.rser.2014.07.155.

[9] IEC 60904-3:2019, Photovoltaic devices–Part 3: measurement principles for terrestrial photovoltaic (PV) solar devices with reference spectral irradiance data, tech. rep, 2019. URL: https://webstore.iec.ch/en/publication/61084, [Online, Accessed on April 21, 2025].

[10] M. Aghaei, A. Fairbrother, A. Gok, S. Ahmad, S. Kazim, K. Lobato, G. Oreski, A. Reinders, J. Schmitz, M. Theelen, P. Yilmaz, J. Kettle, Review of degradation and failure phenomena in photovoltaic modules, Renewable and Sustainable Energy Reviews 159 (2022) 112160. doi:10.1016/j.rser.2022.112160.

[11] L. Osorio, M. Moreno, M. Rivera, V. Tuninetti, G. R. Chavarria, L. Duchêne, P. Wheeler, A metaheuristic-based method for photovoltaic temperature computation under tropical conditions, Solar Energy 271 (2024) 112414. doi:10.1016/j.solener.2024.112414.

[12] S. R. Díaz, A generalized theoretical approach for solar cells fill factors by using Shockley diode model and Lambert W-function: A review comparing theory and experimental data, Physica B: Condensed Matter 624 (2022) 413427. doi:10.1016/j.physb.2021.413427.

[13] A. Zanatta, The Shockley–Queisser limit and the conversion efficiency of silicon-based solar cells, Results in Optics 9 (2022) 100320. doi:10.1016/j.rio.2022.100320.

[14] P. Ferrada, D. Olivares, V. del Campo, A. Marzo, F. Araya, E. Cabrera, J. Llanos, J. Correa-Puerta, C. Portillo, D. Román Silva, M. Trigo-Gonzalez, J. Alonso-Montesinos, G. López, J. Polo, F. J. Batlles, E. Fuentealba, Physicochemical characterization of soiling from photovoltaic facilities in arid locations in the Atacama Desert, Solar Energy 187 (2019) 47–56. doi:10.1016/j.solener.2019.05.034.

[15] D. Olivares, P. Ferrada, J. Bijman, S. Rodríguez, M. Trigo-González, A. Marzo, J. Rabanal-Arabach, J. Alonso-Montesinos, F. J. Batlles, E. Fuentealba, Determination of the Soiling Impact on Photovoltaic Modules at the Coastal Area of the Atacama Desert, Energies 13 (2020). doi:10.3390/en13153819.

[16] D. Olivares, P. Ferrada, A. Marzo, J. Llanos, C. Miranda-Ostojic, V. del Campo, S. Bravo, E. Fuentealba, Microstructural analysis of the PV module cementation process at the Solar Platform of the Atacama Desert, Solar Energy Materials and Solar Cells 227 (2021) 111109. doi:10.1016/j.solmat.2021.111109.

[17] R. R. Cordero, A. Damiani, D. Laroze, S. MacDonell, J. Jorquera, E. Sepúlveda, S. Feron, P. Llanillo, F. Labbe, J. Carrasco, J. Ferrer,

G. Torres, Effects of soiling on photovoltaic (PV) modules in the Atacama Desert, Scientific Reports 8 (2018) 13943. doi:10.1038/s41598-018-32291-8.

[18] P. Tobosque, P. Arriagada, M. Maril, C. Salvo, G. Cabello-Guzmán, E. Astaburuaga, L. Morán, C. Carrasco, Extreme arid conditions: Association among soiling characteristics, transmittance loss and climatic conditions, Solar Energy 240 (2022) 13–26. doi:10.1016/j.solener.2022.05.020.

[19] M. C. Peel, B. L. Finlayson, T. A. McMahon, Updated world map of the Köppen-Geiger climate classification, Hydrology and Earth System Sciences 11 (2007) 1633–1644. doi:10.5194/hess-11-1633-2007.

[20] A. Fezzani, M. I. Hadj, S. Drid, Z. Layachi, B. Abdelhak, B. Messaouda, O. S. Hamid, Degradation and performance evaluation of pv module in desert climate conditions with estimate uncertainty in measuring, Serbian Journal of Electrical Engineering 14 (2017) 277–299. doi:10.2298/SJEE1702277F.

[21] B.-E. Bayandelger, Degradation rate and mechanisms of PV modules in the Gobi Desert of Mongolia after 14 years operated in the field, in: 7th National Renewable Energy Forum-2017, volume 6, 2017, p. 5.

[22] I. H. Mahammed, S. B. Amar Hadj Arab, Y. Bakelli, Impact of the desert climate on the degradation of photovoltaic modules characteristics: a case study, Energy Sources, Part A: Recovery, Utilization, and Environmental Effects 44 (2022) 6021–6034. doi:10.1080/15567036.2022.2091688.

[23] X. Huang, H. Wang, X. Jiang, H. Yang, Performance degradation and reliability evaluation of crystalline silicon photovoltaic modules without and with considering measurement reproducibility: A case study in desert area, Renewable Energy 219 (2023) 119421. doi:10.1016/j.renene.2023.119421.

[24] M. Dahesh, M. Al-Matwakel, M. Dhamrin, Degradation Analysis of 38-Year-Old PV Modules Under the Weather Conditions of Sana'a-Yemen, IEEE Journal of Photovoltaics 15 (2025) 137–145. doi:10.1109/JPHOTOV.2024.3483260.

[25] N. Kahoul, H. Cheghib, M. S. de Cardona, B. C. Affari, M. Younes, Z. Kherici, Performance degradation analysis of crystalline silicon solar cells in desert climates, Energy for Sustainable Development 65 (2021) 189–193. doi:10.1016/j.esd.2021.10.010.

[26] D. Hassan Daher, L. Gaillard, C. Ménézo, Experimental assessment of long-term performance degradation for a PV power plant operating in a desert maritime climate, Renewable Energy 187 (2022) 44–55. doi:10.1016/j.renene.2022.01.056.

[27] A. Bouaichi, A. Alami Merrouni, C. Hajjaj, C. Messaoudi, A. Ghennioui, A. Benlarabi, B. Ikken, A. El Amrani, H. Zitouni, In-situ evaluation of the early PV module degradation of various technologies under harsh climatic conditions: The case of Morocco, Renewable Energy 143 (2019) 1500–1518. doi:10.1016/j.renene.2019.05.091.

[28] B. Adothu, S. Kumar, J. J. John, G. Oreski, G. Mathiak, B. Jäckel, V. Alberts, J. B. Jahangir, M. A. Alam, R. Gottschalg, Comprehensive review on performance, reliability, and roadmap of c-Si PV modules in desert climates: A proposal for improved testing standard, Progress in Photovoltaics: Research and Applications 32 (2024) 495–527. doi:10.1002/pip.3827.

[29] IEC 60891:2021, Photovoltaic devices - Procedures for temperature and irradiance corrections to measured I-V characteristics, 2021. URL: https://webstore.iec.ch/en/publication/61766, [Online, Accessed on April 18, 2025].

[30] C. R. Osterwald, T. J. McMahon, History of accelerated and qualification testing of terrestrial photovoltaic modules: A literature review, Progress in Photovoltaics: Research and Applications 17 (2009) 11–33. doi:10.1002/pip.861.

[31] P. Vásquez, I. Devoto, P. Ferrada, A. Taquichiri, C. Portillo, R. Palma-Behnke, Inspection Data Collection Tool for Field Testing of Photovoltaic Modules in the Atacama Desert, Energies 14 (2021). doi:10.3390/en14092409.

[32] J. Ascencio-Vásquez, J. C. Osorio-Aravena, K. Brecl, E. Muñoz-Cerón, M. Topič, Typical Daily Profiles, a novel approach for photovoltaics performance assessment: Case study on large-scale systems in Chile, Solar Energy 225 (2021) 357–374. doi:10.1016/j.solener.2021.07.007.

[33] A. Abdallah, M. Abdelrahim, M. Elgaili, M. Pasha, K. Mroue, A. Abutaha, Degradation of photovoltaic module backsheet materials in desert climate, Solar Energy Materials and Solar Cells 277 (2024) 113118. doi:10.1016/j.solmat.2024.113118.

[34] A. Bouaichi, P.-O. Logerais, A. El Amrani, A. Ennaoui, C. Messaoudi, Comprehensive analysis of aging mechanisms and design solutions for desert-resilient photovoltaic modules, Solar Energy Materials and Solar Cells 267 (2024) 112707. doi:10.1016/j.solmat.2024.112707.

[35] N. Ammari, M. Mehdi, A. Alami Merrouni, A. Benazzouz, E. Chaabelasri, In-situ soiling evaluation and cleaning schedules optimization for several PV technologies under desert climate, Renewable Energy 224 (2024) 120167. doi:10.1016/j.renene.2024.120167.

[36] M. Alzahrani, T. Rahman, M. Rawa, A. Weddell, Impact of dust and tilt angle on the photovoltaic performance in a desert environment, Solar Energy 288 (2025) 113239. doi:10.1016/j.solener.2025.113239.

[37] R. Shenouda, M. S. Abd-Elhady, H. A. Kandil, A review of dust accumulation on PV panels in the MENA and the Far East regions, Journal of Engineering and Applied Science 69 (2022) 8. doi:10.1186/s44147-021-00052-6.

[38] I. Romero-Fiances, A. Livera, M. Theristis, G. Makrides, J. S. Stein, G. Nofuentes, J. de la Casa, G. E. Georghiou, Impact of duration and missing data on the long-term photovoltaic degradation rate estimation, Renewable Energy 181 (2022) 738–748. doi:10.1016/j.renene.2021.09.078.

[39] J. R. Angulo, B. X. Calsi, L. A. Conde, J. A. Guerra, E. Muñoz, J. de la Casa, J. A. Töfflinger, Estimation of the effective nominal power of a photovoltaic generator under non-ideal operating conditions, Solar Energy 231 (2022) 784–792. doi:10.1016/j.solener.2021.12.015.

[40] J. R. Angulo, L. A. Conde, V. Pleshcheva, M. A. García, W. Gosgot, M. Barrena, E. Muñoz-Cerón, J. de la Casa, J. A. Töfflinger, Effective DC power rating of PV arrays under challenging operating conditions in desert and tropical regions, Renewable Energy 258 (2026) 124981. doi:10.1016/j.renene.2025.124981.

[41] A. Marzo, P. Ferrada, F. Beiza, P. Besson, J. Alonso-Montesinos, J. Ballestrín, R. Román, C. Portillo, R. Escobar, E. Fuentealba, Standard or local solar spectrum? Implications for solar technologies studies in the Atacama desert, Renewable Energy 127 (2018) 871–882. doi:10.1016/j.renene.2018.05.039.

[42] A. M. Gabor, R. Janoch, A. Anselmo, J. L. Lincoln, H. Seigneur, C. Honeker, Mechanical Load Testing of Solar Panels – Beyond Certification Testing, in: 2016 IEEE 43rd Photovoltaic Specialists Conference (PVSC), 2016, pp. 3574–3579. doi:10.1109/PVSC.2016.7750338.

[43] R. Singh, M. Sharma, K. Yadav, Degradation and reliability analysis of photovoltaic modules after operating for 12 years: A case study with comparisons, Renewable Energy 196 (2022) 1170–1186. doi:10.1016/j.renene.2022.07.048.

[44] E. Adıgüzel, 10 year performance and degradation analysis of different photovoltaic panels in the Istanbul Türkiye environment, Renewable Energy 251 (2025) 123327. doi:10.1016/j.renene.2025.123327.

[45] M. Islam, M. Hasanuzzaman, N. A. Rahim, A comparative investigation on in-situ and laboratory standard test of the potential induced degradation of crystalline silicon photovoltaic modules, Renewable Energy 127 (2018) 102–113. doi:10.1016/j.renene.2018.04.051.

[46] M. Ángel Sevillano-Bendezú, L. Ángel Conde, M. A. García, J. R. Angulo, J. de la Casa, J. M. Ripalda, J. A. Töfflinger, Performance loss rate and benchmarking of c-Si and thin-film PV modules considering thermal and spectral effects at a low-latitude site, Renewable Energy 257 (2026) 124732. doi:10.1016/j.renene.2025.124732.